# *Drosophila* ryanodine receptor gene triggers functional and developmental muscle properties and could be used to assess the impact of human *RYR1* mutations

*Monika Zmojdzian [1,2]*, Teresa Jagla [1]*, Florian Cherik [2], Magda Dubinska-Magiera [3], Marta Migocka-Patrzalek [3], Malgorzata Daczewska [3], John Rendu [4], Krzysztof Jagla [1,5] and Catherine Sarret [1,2,5]*

Affiliations:

[1] Institute of Genetics Reproduction and Development, INSERM U1103, CNRS UMR6293, Université Clermont Auvergne, 28 place Henri-Dunant, 63001 Clermont-Ferrand, France

[2] Reference Centre for Neuromuscular Disorders, Department of Medical Genetics, Hôpital Estaing, CHU Clermont-Ferrand, 63000 Clermont-Ferrand, France

[3] Department of Animal Developmental Biology, Faculty of Biological Sciences, University of Wroclaw, Sienkiewicza 21, 50-335 Wrocław, Poland

[4] Université Grenoble Alpes, INSERM U1216, CHU Grenoble Alpes, Grenoble Institute Neurosciences, 38000 Grenoble, France

* equal contribution

[5] correspondence to: csarret@chu-clermontferrand.fr; christophe.jagla@uca.fr

## ABSTRACT

The ryanodine receptor (RYR) genes encode evolutionarily conserved calcium release channels involved in a wide range of calcium-dependent biological processes. Here we show that the sole *Drosophila* RYR gene (*dRyR*) functions in differentiated somatic and cardiac muscle as well as in developing embryonic myotubes. In the larval body wall muscles, dRyR protein localizes at the SR membranes and *dRyR* knockdown adversely affects muscle contractility, suggesting its conserved role in calcium-triggered E-C coupling. After *dRyR* attenuation, sarcomere and mitochondrial patterns are severely impaired, showing *dRyR* involvement in structural muscle properties. However, *dRyR* is also prominently expressed and functionally required in growing embryonic muscles. *dRyR* loss of function leads to myotube growth defects and thin myofiber phenotypes, while its overexpression induces myofiber splitting. Given the structural and functional conservation of *dRyR*, we used *Drosophila* to test the impact of one human *RYR1* variant of unknown significance (VUS). Larvae carrying *p.Met4881Ile RYR1* VUS showed impaired mobility and altered structural muscle properties reminiscent of those seen in *dRyR* knockdown, thus indicating it is likely pathogenic. Overall, we show that *Drosophila dRyR* plays a conserved role in setting muscle contractility and structural muscle features. Our findings underline the still under-investigated role of *dRyR* as a promyogenic factor and provide a first example of the impact assessment of a human *RYR1* VUS in *Drosophila*.

## Introduction

The calcium ion ($Ca^{2+}$) concentration gradient is known to be a crucial second messenger signal in all eukaryotic cells. The calcium release channels encoded by ryanodine receptor genes are essential to maintaining correct $Ca^{2+}$ dynamics across biological membranes. RYR proteins are cellular sites of interactions with ryanodine, an alkaloid isolated from the stem wood of the plant *Ryania speciosa* (Jenden and Fairhurst, 1969) that was used for several decades as an insecticide. Because of its muscle-paralyzing effect in humans, ryanodine has been replaced by insect-specific derivatives that are non-toxic for mammals. Analysis of the RYR multi-domain structures and phylogenetic relations among different taxa yields a model suggesting that it evolved from inositol 1,4,5-trisphosphate receptor ($IP_3R$)-like ancestral $Ca^{2+}$ release channels. The RYR activity is strictly controlled and may respond to the presence of ions ($Ca^{2+}$, $Mg^{2+}$, and $Zn^{2+}$), proteins (calmodulin (Cam) and FK-506 binding protein (FKBP12/12.6)), and small molecules such as ATP, caffeine, and ryanodine. The domain structure is highly conserved. For example, the SPIa kinase and ryanodine receptor (SPRY) domain shares high sequence identity between vertebrates and invertebrates and is engaged in protein-protein interactions with several protein families (Hadiatullah et al., 2022).

The number of RYR copies ranges across taxa. Mammalian genomes carry three RYR genes. For example, in humans, *RYR1*, *RYR2* and *RYR3* are located on chromosomes 19q13.2, 1q43 and 15q13.3-14, respectively. Non-mammalian vertebrates, such as *Xenopus laevis* and chicken, have two *RYR* copies (Ottini et al., 1996) while in a zebrafish genome, there are five genes: *RYR1a, RYR1b, RYR2a, RYR2b*, and *RYR3* displaying high similarity to other vertebrate RYR genes (Wu et al., 2011). The greater number of RYR genes in zebrafish than in mammals and birds is thought to result from teleost-specific whole-genome duplication (Howe et al., 2013; Postlethwait et al., 1998). In the invertebrates *Drosophila melanogaster*, *Caenorhabditis elegans,* live scallop (*Placopecten magellanicus*), and lobster (*Homarus americanus*), a single RYR gene has been identified (Hasan and Rosbach, 1992; Maryon et al., 1996; Murayama & Kurebayashi, 2011; Quinn et al., 1998, Xu et al., 2000). However, through alternative splicing, the single invertebrate RYR gene produces several isoforms, thus increasing the diversity of the available protein pool (De Mandal et al., 2019; George et al., 2007).

It is well known that RYR genes are expressed in muscle cells and play a crucial role in muscle contraction, which results from excitation-contraction (E-C) coupling, a series of events involving the conversion of electrical stimulus to Ca-dependent mechanical response. However, RYRs are also expressed in many other animal tissues including the central nervous system (Klatt Shaw et al., 2018; Q. Liu et al., 2005) and are involved in housekeeping functions in the cells of the adult organism and in developmental processes (Fill & Copello, 2002).

*RYR1* mutations underlie an array of diseases including muscle-impairing central core disease (CCD), one of the most frequent congenital myopathies, and malignant hyperthermia susceptibility (MHS), characterized by severe reaction to anesthetics, excessive heat or exercise, which can be fatal.

In addition, several *RYR2* mutations have also been implicated in cardiopathic catecholaminergic polymorphic ventricular tachycardia (CPVT) and arrhythmogenic right ventricular dysplasia of type 2 (ARVD2) (Lanner, 2012). Of the numerous mutations identified to date in RYR genes, most are missense mutations with single amino acid substitutions. However, several deletions, duplications and frame shift mutations have also been identified (Lanner, 2012).

Here, we analyze the phylogenetic origin, expression and function of the *Drosophila* dRyR gene. Our data show that *dRyR* is not only required for contractile properties of differentiated somatic and cardiac *Drosophila* muscle but also influences muscle structure and plays an instructive role in muscle development. Structural muscle changes in a *dRyR* loss-of-function context suggest its implication in age-associated muscle decline, while severe developmental muscle defects observed in *dRyR* mutant embryos provide insights into early-onset RYR-related myopathies. Considering extensive structural and functional *dRyR* conservation, we generated a *Drosophila* model of one undiagnosed human *RYR1* variant mutation (*p.M4881Ile*) and found that it negatively impacted muscle structure and function, making it likely pathogenic. We report a detailed functional analysis of *dRyR*. Our findings pinpoint the under-investigated role of *dRyR* in embryonic muscle development and demonstrate that *Drosophila* could be used for assessing impacts of human *RYR1* variant mutations of unknown significance.

## Results

### *Drosophila dRyR* belongs to the RYR gene family and shows conserved somatic and cardiac muscle-associated expression and function

*dRyR* is the sole RYR gene family member in *Drosophila*. We applied the maximum likelihood method and the Kimura 2-parameter model (Kimura, 1980) to infer the evolutionary history of *dRyR*. Based on evolutionary distance studies, *RYR2* is the most ancient of three human RYR genes (Ding et al., 2017) and shows the highest sequence homology with *Drosophila dRyR*. We compared sequences of *RYR2* from selected mammalian and non-mammalian vertebrates with the sequence of single invertebrate RYR, including fruit fly *dRyR* to illustrate its phylogenetic origin (Fig. 1A) (Ding et al., 2017; Mackrill, 2012; McKay & Griswold, 2014; Takeshima et al., 1994). Evolutionary analyses were conducted in MEGA X (Kumar et al., 2018; Stecher et al., 2020). We observed that single invertebrate RYR genes, here from *Drosophila* and *C. elegans*, clustered into a separate branch connected to the vertebrate *RYR2* branch that clustered 100% (Fig. 1A). The vertebrate *RYR2* branch was then subdivided clonally from *Xenopus* through zebrafish, chick and mouse to human. All clonal branches in vertebrates clustered 100% (Fig. 1A), indicating that *RYR2* genes are closely related and most probably evolved from a single invertebrate RYR.

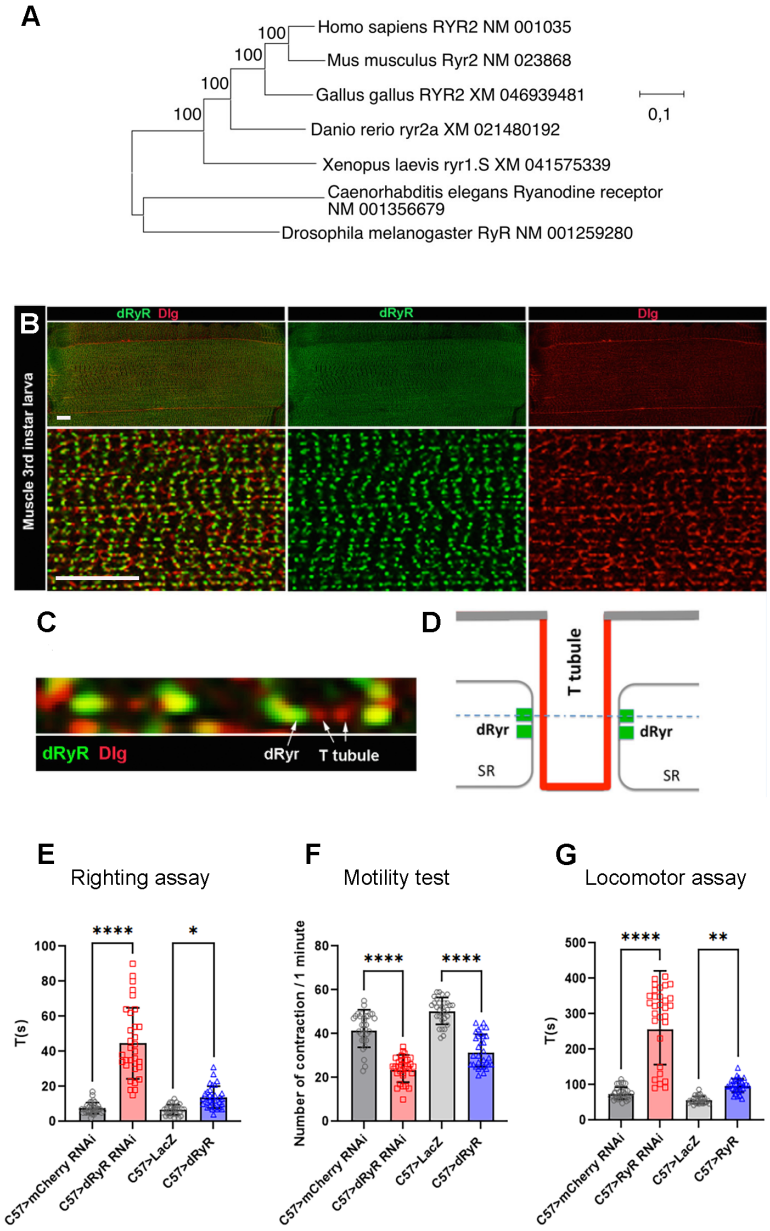


**Figure 1.** ***Phylogenetic origin of dRyR, its body wall muscle associated expression and role in locomotion.*** (A) Evolutionary analysis by the maximum likelihood method of ryanodine receptor genes (RYR) from different taxa. The tree with the highest log likelihood (−95718.65) is shown. The percentage of trees in which the associated taxa clustered is shown next to the branches. (B) A wide view (upper panels) and a zoomed view (lower panels) of ventral VL3 larval muscle stained for dRyR (green) and Dlg (red) that labels T-tubules. (C) A high-magnification view showing dRyR dots at the interface of T-tubules (arrows). (D) Scheme presenting subcellular location of dRyR receptor at the sarcoplasmic reticulum (SR) membrane in a close vicinity of T-tubules. The dotted line refers to the optical level of confocal view in (C). (E-G) Larval muscle targeted *dRyR* knockdown (C57>dRyRRNAi) leads to a marked decline in muscle performance compared to control (C57>mCherryRNAi). Three muscle performance tests were applied: (E) righting test, (F) motility test, and (G) locomotor test. Overexpression of *dRyR* in larval muscle (C57>dRyR) impacts muscle performance measured by the locomotor and motility tests (F, G). Scale bar: 20 μm. All statistical analyses were performed using Prism. The one-way ANOVA test was used for comparisons of datasets. Bar plot represent the mean and the standard deviation. On the figures, statistical comparisons of sample vs control are indicated as ****: P ≤ 0.0001; ***: P ≤ 0.001; **: P ≤ 0.01; *: P ≤ 0.05; ns > 0.05.

Expression of RYR genes in vertebrates has been extensively studied and described in various excitable cells including skeletal and cardiac muscles and neurons, and in non-excitable cells such as pancreatic beta cells and lymphocytes (Rossi & Sorrentino, 2002). By contrast, in spite of early works by Hasan and Rosbash (1992) and Sullivan et al., (2000) no systematic analyses have yet been performed to assess the developmental expression pattern of the sole *Drosophila dRyR* gene.

We first tested the expression of *dRYR* at protein level. In differentiated body wall muscle of 3rd instar larva (Fig. 1B,C) *dRyR* was detected in a discrete striated pattern (Fig. 1B), which in a zoom view revealed highly ordered punctate dRyR protein localization in close vicinity to discs large (Dlg)-positive T-tubules (Fig. 1C and scheme in Fig. 1D). Thus, in *Drosophila* muscle, like in vertebrates, dRyR localizes at the T-tubule interface, a sub-cellular localization consistent with its calcium release role at SR and E-C coupling function during muscle contraction.

We also assessed muscle-associated expression of *dRyR* transcripts (Fig. S1). Of ten *dRyR* transcript isoforms, all coded for proteins of similar amino acid (aa) length, ranging from 5113 to 5134 aa and molecular weight about 580 kDa (http://flybase.org/reports/FBgn0011286.htm). To test *dRyR* isoform expression, we applied the FISH-HCR technique (Choi et al., 2016) and four probes targeting alternative exons 10, 11, 22 and 23 (Fig. S1A). In this setup we detected the expression of the A,B,F,G,H,J isoforms with the *dRyR* Ex10 probe, A,B,C,D,E,I isoforms with the Ex11 probe, A,B,C,D,E,F,G isoforms with the Ex22 probe and H,I,J isoforms with the Ex23 probe (Fig. S1A).

FISH-HCR experiments performed on differentiated 3rd instar larval muscles revealed muscle-associated specific signals with all four probes (Fig. S1B-E'). *dRyR* transcripts were detected at the periphery of nuclei, in the sarcoplasm and in a repeated striated pattern following sarcomeres. Similar signals observed with the four probes indicated that at least the isoforms A and B that are commonly targeted by the Ex10, Ex11 and Ex22 probes and one of the isoforms H,I or J targeted by the Ex23 probe were present in the functional body wall muscle. We could not, however, rule out the possibility that most or even all *dRyR* isoforms were expressed in the differentiated body wall muscles. Supporting this, we note that nine out of ten *dRyR* isoforms (isoform I being an exception) share the same transcription start site, suggesting that a common core promoter regulates their expression.

Detected muscle-associated expression of *dRyR* prompted us to test its involvement in muscle contraction and larva mobility. We observed that muscle-targeted attenuation of *dRyR* expression resulted in reduced muscle performance with a significantly longer time required for larvae to switch from the dorsal to the ventral position (Fig. 1E – righting test) and a reduced number of muscle contraction waves compared to control recorded in 1 minute (Fig. 1F – motility test).

Finally, *dRyR-RNAi* larvae crawled inefficiently and were unable to move over a longer distance (Fig. 1G – locomotor test). In parallel, overexpressing *dRyR* in larval muscles also impaired muscle function, with fewer contraction waves in 1 minute compared to control and a slower locomotion (Fig. 1F,G), while the time required to switch from the dorsal to the ventral position remained unchanged (Fig. 1E).

Altogether, our data extend previous observations of affected muscle contractility in RyR mutants (Sullivan et al., 2000) and suggest that *Drosophila dRyR*, like its vertebrate counterparts, ensures correct muscle function, likely acting as a sarcoplasmic reticulum (SR) calcium release channel essential for muscle contraction and E-C coupling.

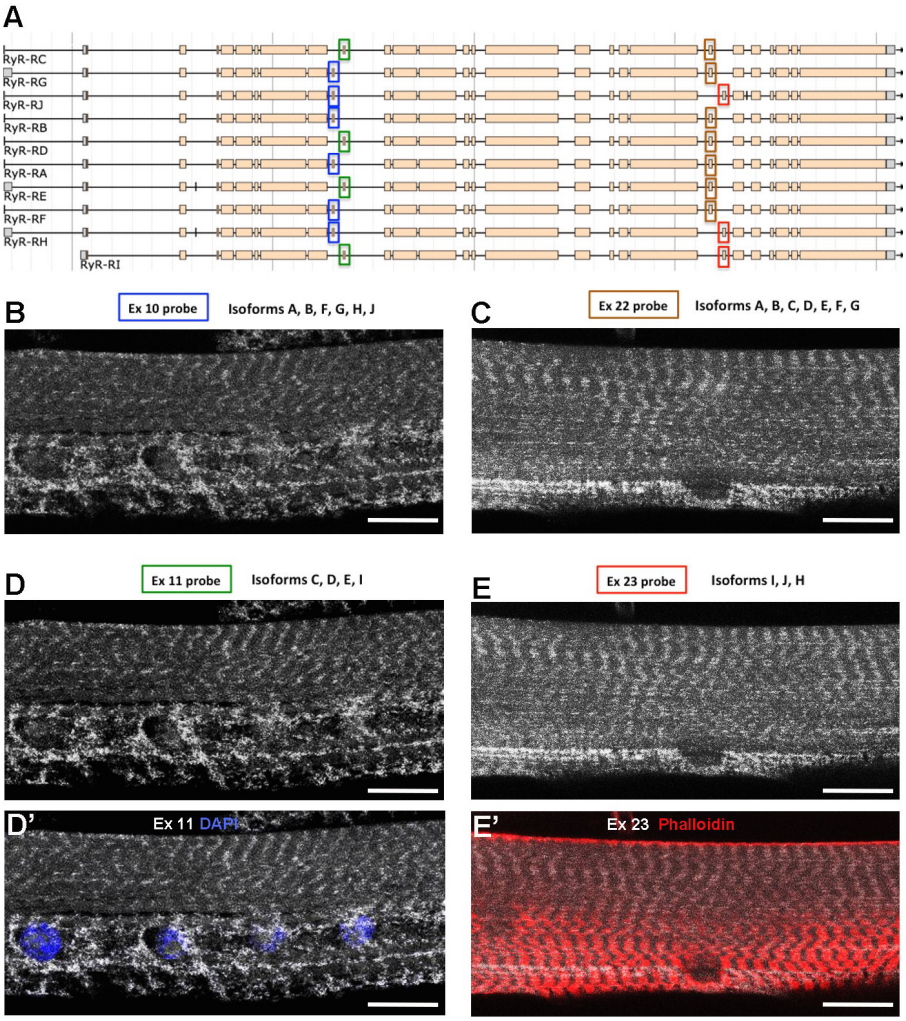


***Figure S1. dRyR transcript expression in larval muscles.*** (A) Exon/intron organization of *dRyR* isoforms. FISH-HCR probes and targeted alternative exons are indicated by boxes with a color code. (B-E) Confocal views of *dRyR* transcript patterns in VL3 larval muscles revealed with FISH-HCR probes (white). Identities of the FISH-HCR probes and targeted *dRyR* isoforms are indicated above panels. Note highly similar subcellular distribution of different *dRyR* transcripts. (D') Exon11 FISH-HCR (white) with nuclear DAPI staining (blue). (E') Exon23 FISH-HCR (white) with phalloidin staining (red) to reveal sarcomeric pattern. Scale bar: 20 μm.

Given that vertebrate RYR genes (*RYR2* in humans) also play an instrumental role in cardiac muscle function, we sought to determine whether dRyR protein could be detected in the fly heart and whether it could influence heartbeat variables. In the adult *Drosophila* heart, dRyR protein was detected predominantly in the circular muscle fibers ensuring cardiac contractions (Fig. 2A-A'''), which appear structurally affected (Fig. 2C, E) in a heart-specific *dRyR RNAi* context (Hand>dRyR RNAi). Consistent with this, heart-targeted attenuation of *dRyR* resulted in an abnormal M-mode heart profile (Fig. 2B,D) associated with a longer heart period (Fig. 2F) and a slow heart rate (Fig. 2G), with significantly increased diastolic interval (Fig. 2H). Attenuation of cardiac *dRyR* expression also led to arrhythmic heartbeat (Fig. 2J), increased systolic diameter (Fig. 2K) and reduced fractional shortening (Fig. 2M). As the diastolic diameter remained unchanged, we conclude that cardiac dRyR knockdown affects cardiac performance without causing dilated cardiomyopathy. In contrast to dRyR-RNAi, increasing *dRyR* cardiac expression had only a minor influence on cardiac variables (Fig. 2F-M) with increased systolic diameter (Fig. 2K) but no effect on cardiac contractility (Fig. 2M). Overall, observed *dRyR* loss-

of-function adult fly heart phenotypes with a slow heart rate and increased arrhythmia correlate with impaired cardiac function in RyR mutant larvae (Sullivan et al., 2000). We hypothesize that dRyR RNAi-induced impairment of Ca2+ homeostasis could contribute to cardiac aging, for which Drosophila is a recognized model (Nishimura et al., 2011).

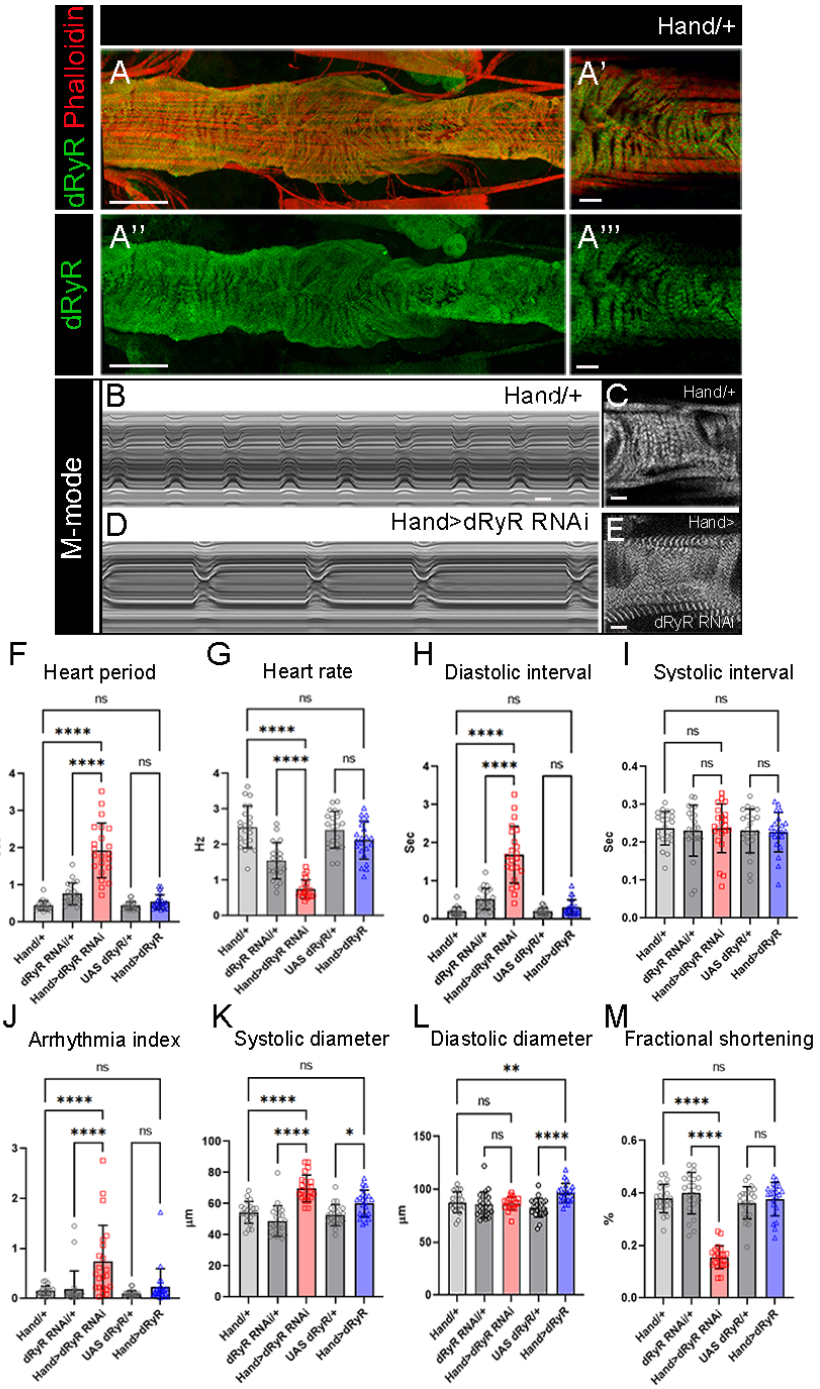


***Figure 2. dRyR is expressed in the heart tube and is required for correct heartbeat.*** **(**A-A'') Adult heart tube labeled for dRyR (green) and actin (red). (A', A''') Zoomed views revealing *dRyR* expression in circular fibers. (B,D) M-modes of control Hand/+ (B) and Hand>dRyR RNAi (D) contexts showing a slow heart rate induced by *dRyR* attenuation. Compared with control (C), circular fibers in Hand>dRyR RNAi (E) context showed a fuzzy pattern suggesting an affected sarcomeric organisation. (F-M) Heartbeat variables in cardiac *dRyR* knockdown (Hand>dRyR RNAi) and cardiac *dRyR* overexpression contexts (Hand>dRyR). Scale bar: 50 µm in A, A''; 10 µm in A', A''', C, E. All statistical analyses were performed using Prism. The one-way ANOVA test was used for comparisons of datasets. Bar plot represent the mean and the standard deviation. On the figures, statistical comparisons of sample vs control are indicated as ****: P ≤ 0.0001 *: P ≤ 0.05; ns > 0.05.

In view of the reduced motility of 3rd instar larva with the attenuated *dRyR* (Fig. 1E-G) we examined whether structural properties of body wall muscles were adversely affected. We first found that muscle-targeted attenuation of *dRyR* (C57>dRyR RNAi) led to a significantly reduced larva body length (Fig. 3B, Q) compared to control (Fig. 3A, Q, an observation that correlates with previously observed (Sullivan et al., 2000) reduced body size of $dRyR^{16}$ mutant larvae. Though to a lesser extent, the overexpression of *dRyR* in body wall muscles also impacted larva length (Fig. 3D, Q). These changes in larva size in loss and gain of *dRyR* function correlated with a reduced longitudinal muscle length (Fig. 3 E-H, R), which in turn correlated with shortening of Kettin/D-Titin-labelled sarcomeres (Fig.3 I-L, T) and reduced number of myonuclei (Fig.3 E-H, S). Because RYR-mediated calcium homeostasis involves dynamic interactions between the sites of calcium release from the SR and calcium uptake by the mitochondria (Li et al., 2025) we examined whether in *Drosophila dRyR* loss and/or *dRyR* gain of function could adversely affect mitochondria pattern in the larval muscles. We noted that the I band-associated striated mitochondria pattern was lost in the C57>dRyR RNAi context (Fig. S2 B) and appeared irregular when *dRyR* was overexpressed in muscles (Fig. S2 D) compared to the wild-type larval muscles (Fig. S2A, B, E).

Both muscle-targeted attenuation and gain of *dRyR* function led not only to impaired muscle functions but also to overall reduction of muscle size and myofibrillar disarray associated with a downsizing of sarcomeres and mitochondrial mismatch. Altered structural muscle features observed in *dRyR*-attenuated *Drosophila* larvae are reminiscent of myofibrillar and mitochondrial pattern defects reported in mice harboring a pathogenic *RYR1* mutation (Elbaz et al., 2019).

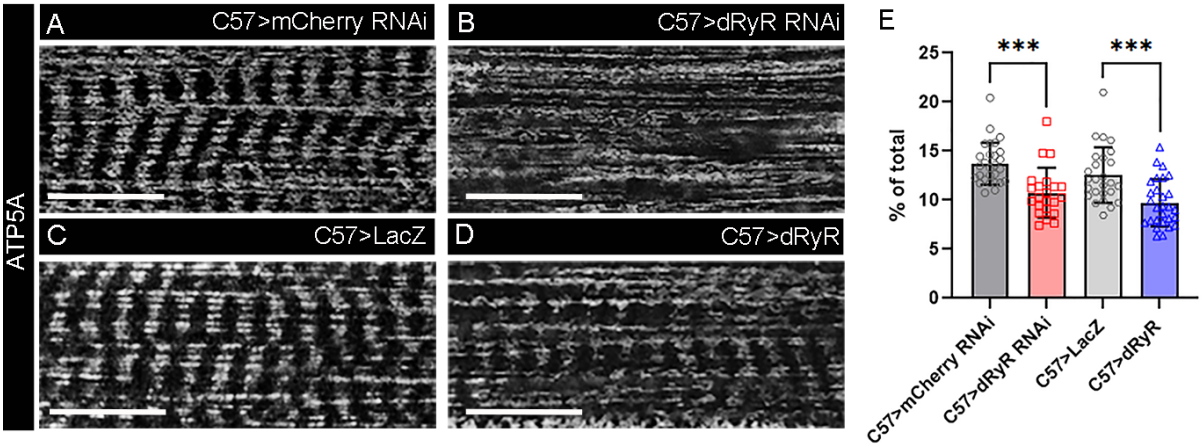


**Figure S2. dRyR is required for correct mitochondria pattern. (**A-D) Zoomed views of a 3rd instar VL3 muscle in control (A, C), muscle-targeted dRyR attenuation (B) or overexpression (D) stained for ATP5 to reveal mitochondria pattern. (E) Statistical representation of ATP5 staining area in control, C57>dRyR RNAi and C57>dRyR contexts. "% of total" means the percentage of the measured muscle area that is positive for ATP5a staining. Scale bar: 20 μm. All statistical analyses were performed using Prism. The one-way ANOVA test was used for comparisons of datasets. Bar plot represent the mean and the standard deviation. On the figures, statistical comparisons of sample vs control are indicated as; ***: $P \leq 0.001$.

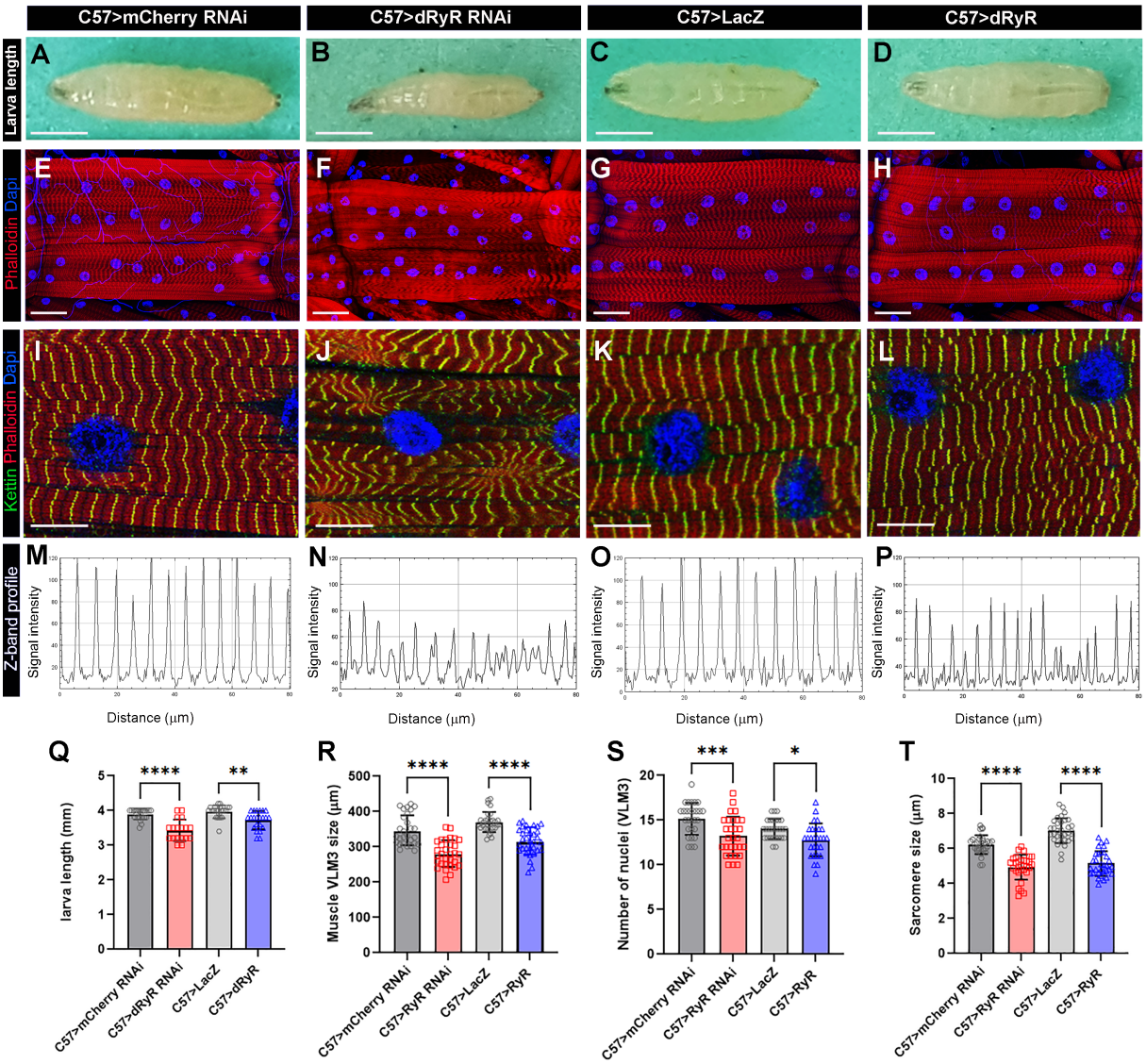


***Figure 3. Muscle targeted dRyR loss and gain of function impacts body size and structural muscle properties.*** **(**A-D) General views of 3rd instar larva in control (A, C), muscle-targeted *dRyR* attenuation (B) or overexpression (D). (E-H) Representative VL3 and VL4 ventral longitudinal muscle views from age-matched 3rd instar larvae in control (E, G), C57>dRyR RNAi (F) and C57>dRyR (H) contexts. Muscle fibers and nuclei were revealed with phalloidin (red) and DAPI (blue), respectively. (I-L) Zoomed views of VL3 muscles of control (I, K), C57>dRyR RNAi (J) and C57>dRyR (L) larvae triple stained for phalloidin (red), DAPI (blue) and Kettin/D-Titin (green). (M-P) Z band profiles (Kettin signal intensity plot) from zoomed views of VL3 muscles presented in (I-L). (Q) Statistical representation of 3rd instar larva length. (R-T) Statistical representation of VL3 muscle characteristics: (R) VL3 muscle length; (S) number of nuclei and (T) sarcomere size. Scale bar: 1 mm in A-C; 50 μm in D-F; 20 μm in G-I. Bar plots represent the mean and the standard deviation. All statistical analyses were performed using Prism. The one-way ANOVA test was used for comparisons of datasets. Bar plot represent the mean and the standard deviation. On the figures, statistical comparisons of sample vs control are indicated as ****: P ≤ 0.0001; ***: P ≤ 0.001; **: P ≤ 0.01; *: P ≤ 0.05; ns > 0.05.

## *dRyR* is expressed during embryonic muscle development and is required for correct myogenic differentiation

Previous reports provide evidence that RYR-dependent elevation of intracellular calcium promotes late steps of myogenic differentiation and in particular fusion of myoblasts to myotubes (Eigler et al., 2021; Sinha et al., 2022). In parallel, a recent study on RYR1-depleted primary myoblasts revealed the calcium-independent inhibitory role of RYR1 in myogenic differentiation (Tourel et al., 2025). To further explore myogenic roles of RYRs, we tested *dRyR* expression and function during embryonic development.

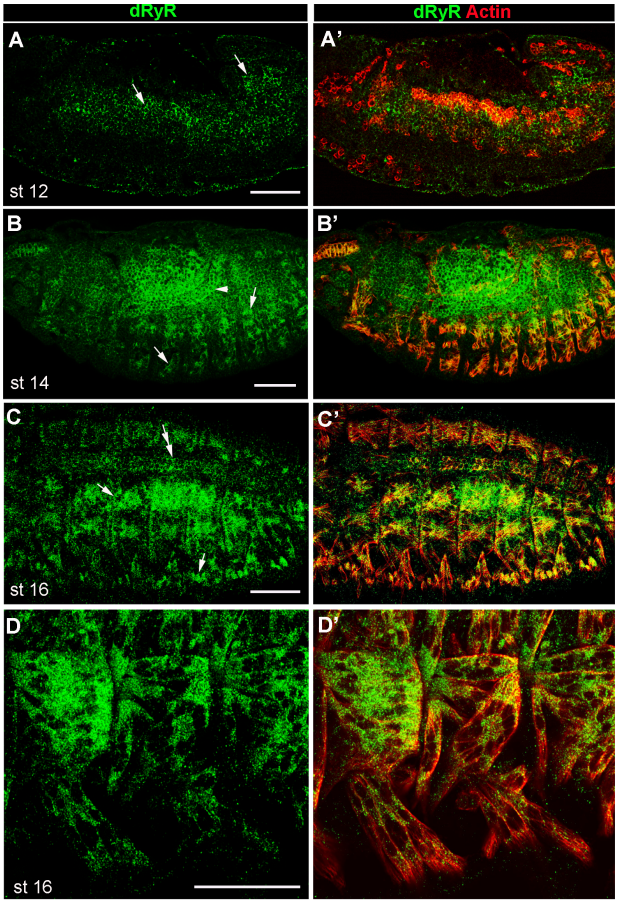


***Figure 4. Developmental dRyR protein pattern in embryos.***
(A-A') lateral view of a stage 12 embryo. dRyR (green) could be detected in the somatic and visceral muscle precursors (arrows in A) also revealed by Actin (red) (A'). (B-C') dorso-lateral views of stage 14 (B,B') and stage 16 (C,C') embryos. dRyR accumulates in body wall muscle precursors (arrows in B and C) and in visceral muscle of the midgut (arrowhead in B) and in the dorsally aligned cardioblasts (double-head arrow in C). (D,D') Subcellular dRyR pattern in ventral muscle precursors at embryonic stage 16. Note granular cytoplasmic distribution of dRyR. Scale bar: 50 μm.

Sullivan et al. (2000) reported embryonic *dRyR* transcript expression in body wall and visceral muscle precursors. Here, we tested dRyR protein expression and found that it was prominently expressed in the mesodermal derivatives in embryos. We detected dRyR protein in the developing visceral, somatic and cardiac muscle cells (Fig. 4). Regarding body wall muscles, dRyR could be detected in the somatic muscle precursors starting from embryonic stage 12 (Fig. 4A, A'), accumulated in the growing myotubes at mid-stage embryos (Fig. 4B, B') and continued to be expressed in the developing muscle fibers at later embryonic stages (Fig. 4C-D'). At embryonic stage 16, dRyR protein was distributed in a discrete granular pattern within the cytoplasm of myofibers and appeared excluded from the myonuclei (Fig. 4D,D'). Thus, dRyR protein was detected from the early phase of myogenic differentiation that encompasses specification of muscle founders and first myoblast fusion events and

continues during the second phase of fusion and myofiber growth and maturation. We also applied HCR-FISH to test *dRyR* transcript isoform expression in the developing somatic muscle (Fig. S3). We found that *dRyR* A, B, F and G isoforms harboring alternative exons 10 and 22 were actively transcribed in the developing muscle, whereas the remaining *dRyR* isoforms were barely detected (Fig. S3).

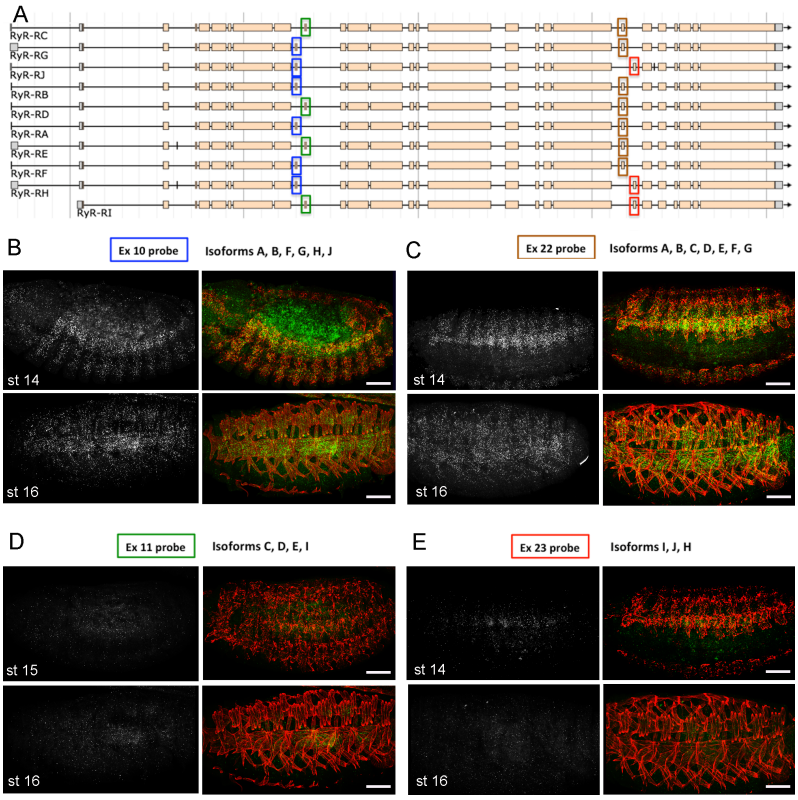


***Figure S3. Embryonic expression of dRyR transcript isoforms.***
**(A)** Exon/intron organization of *dRyR* isoforms. Blue, green, brown and red boxes indicate alternative exons 10, 11, 22 and 23 (FISH-HCR probes). (B-E) Representative views of stage 13 and stage 16 embryos stained for four FISH-HCR probes (white/green) and actin (red) to reveal somatic muscles. Note that Ex10 and Ex22 probes consistently labeled *dRyR* transcript isoforms listed at the top of panels that accumulate in the developing muscle precursors. No or only faint *dRyR* expression was detected with Ex11 and Ex23 probes. Scale bar: 50 μm.

Previous analyses (Sullivan et al., 2000) showed that muscle contraction was compromised in larvae carrying a hypomorphic $dRyR^{16}$ mutant allele. *dRyR* mutant larvae were also smaller in size and died before the pupation stage. However, whether *dRyR* embryonic expression has a functional impact on larval muscle development has not yet been assessed. Accordingly, we analyzed embryonic muscle pattern in late-stage $dRyR^{16}$ mutant embryos (Fig. 5). We observed a wide range of developmental somatic muscle defects with predominant phenotype of thin myofibers present in 64% of abdominal A2-A5 hemisegments and more severely sphere-shaped (arrowheads in Fig. 5B) or missing myofibers (asterisks in Fig. 5B) observed in 25% of hemisegments. In addition, in 10% of hemisegments with *dRyR* loss of function led to supernumerary lateral transverse (LT) muscles (arrows in Fig. 5B), a phenotype that could arise from LT muscle splitting (Bertin et al., 2021). Predominant thin/misshaped/missing myofiber phenotype in a *dRyR* loss-of-function context suggests a pro-myogenic role during development. To further characterize the role of dRyR during myogenesis, we analyzed embryonic LT muscle phenotypes in LT-targeted *dRyR* attenuation and gain-of-function contexts (Fig. 5C-E). Like in $dRyR^{16}$ mutant embryos, *dRyR* RNAi knockdown in LT muscles resulted in thin and/or misshaped LT muscles (Fig. 5D, H) observed in 88% of hemisegments and in rare cases of LT splitting, found in 8% of hemisegments (Fig. 5D, H). We noted no loss of LT muscles in *dRyR* RNAi embryos. Consistent with the promyogenic role of *dRyR*, LT-targeted overexpression of *dRyR* appears to promote LT splitting phenotype (Fig. 5E, H) found in 18% of hemisegments. Calmodulin (Cam is the major calcium

dependent RYR regulator. The Ca2+-bound Cam at high calcium levels acts as RYR inhibitor (Fruen et al., 2003). We thus tested effects of Cam attenuation in LTs and found that it results in a dRyR overexpression-like phenotype (Fig. 5F, H). This suggests that during myogenesis Cam is present mainly in a calcium-bound form that represses dRyR. Another major regulator of calcium homeostasis, the endoplasmic reticulum calcium pump SERCA is required to maintain a high calcium levels in the ER lumen (Suisse & Treissman, 2019). To test its role in myogenesis we analysed Lms>SERCA RNAi embryos. We observe that SERCA-depleted LT muscles display growth defects with predominant thin myofiber phenotype (Fig. 5G, H) also observed in Lms>dRyR RNAi context (Fig. 5D, H). Thus, both dRyR-regulated cytosolic and SERCA-regulated ER lumen calcium levels are required to promote muscle development.

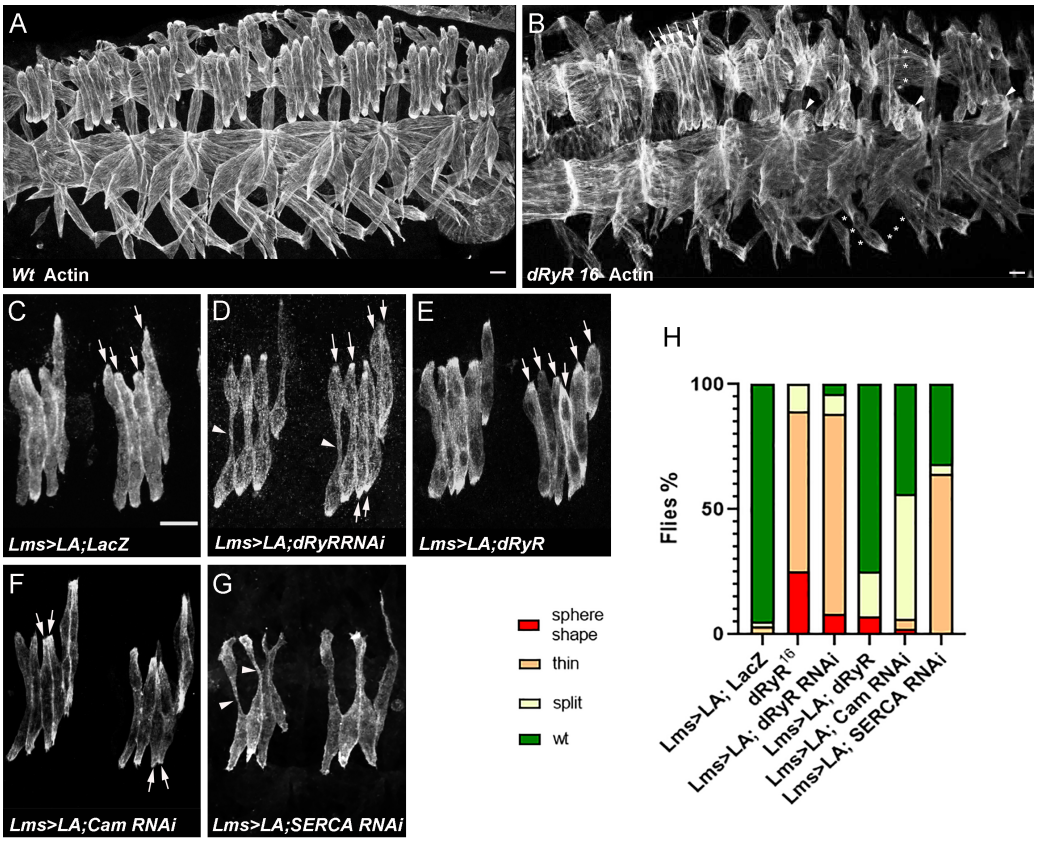


***Figure 5. dRyR is required for correct embryonic muscle development.*** (A, B) ventro-lateral views of stage 16 embryos stained for actin to reveal embryonic muscle pattern in wild-type (A) and in homozygous *dRyR*$^{16}$ mutant embryo (B). Note a wide range of developmental muscle defects that could be observed in *dRyR* loss-of-function context. Asterisks in B pinpoint muscle fiber loss, arrowheads indicate the myofibers that failed to extend and remained as myospheres and a series of arrows point to supernumerary lateral transverse myofibers (6 instead of 4). (C-E) Effects of lateral transverse (LT) muscle-targeted attenuation (D) and overexpression (E) of *dRyR*. LT muscles were revealed by targeted expression of LifeActinGFP (LA) transgene using LT-specific Lms-GAL4 driver. (C) Four LT muscles (arrows) are seen in a control Lms>LA;LacZ context. (D) dRyRRNAi attenuation led to misshaped thin LTs (arrowheads) – major phenotype and to an occasional LT muscle split phenotype (6 LTs indicated by arrows). (E) LT targeted overexpression of *dRyR* resulted mainly in LT muscle splitting (arrows). (F) Cam attenuation induced mostly LT muscle splitting (arrows) while (G) SERCA RNAi knockdown lead to affected myofiber growth with thin LT muscle phenotype (arrowheads). (H) Statistical representation of LT muscle phenotypes in *dRyR* mutants and LT targeted *dRyR* knockdown, gain-of-function and Cam and SERCA attenuation contexts. The statistical analyses were performed using Prism - contingency test; 50-60 segments/genotype. Scale bar: 10 μm.

Interestingly, live imaging (Fig. S4) shows that the sphere-shaped muscle phenotype arises from the impaired LT myotube extension and not from retraction of already extended myotubes. Also myonuclei remained on LT extremities and did not spread along the abnormally thin myofibers. The reduced number of myonuclei (2-4 per dRyR RNAi LT myofiber (Fig. S4B, lower panel) instead of 4-6 in control LTs (Fig. S4A lower panel)) points to the role of *dRyR* in the second wave of fusion (Eigler et al., 2021). This observation is consistent with the fact that overexpression of *dRyR* induced the LT split phenotype (Fig. 4E) known to be promoted by an excessive myoblast fusion (Bertin et al., 2021). Because the embryonic LT muscle defects in *dRyR*-mutant embryos are associated with a reduced calcium signal in LTs (Fig. S4 C, D), we hypothesize that *dRyR* acts as a promyogenic factor ensuring correct calcium levels in the developing myotubes.

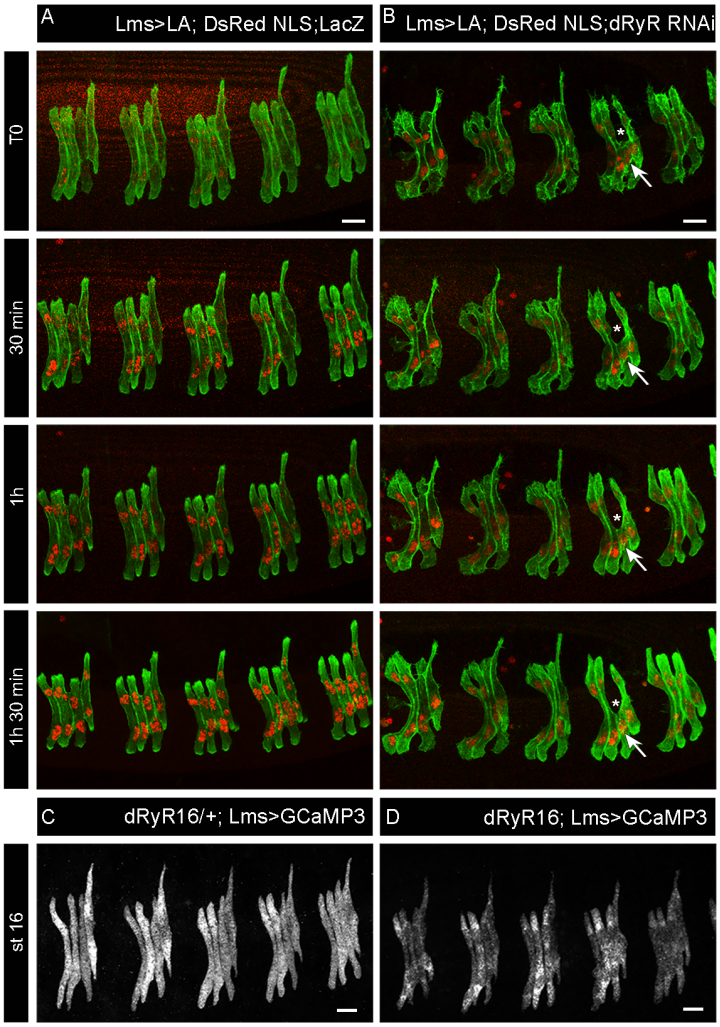


***Figure S4. Live imaging of developing LT muscles and GCAMP-revealed calcium levels in control and dRyR loss-of-function contexts.***Time-lapse images of developing LT muscles revealed by LifeActin-GFP (green) and myonuclei revealed by DsRed NLS (red) in (A) control Lms>LA; DsRed NLS; LacZ and (B) Lms>LA; DsRed NLS; dRyR RNAi embryos. (B) Arrows point to a growth-defective LT3 muscle and asterisks show the area where it is missing within the segment. Note a reduced myonuclei signal in dRyR RNAi context compared to control (red staining) indicating fewer myonuclei in LTs after *dRyR* attenuation.
(C-D) Representative lateral views of LT muscles from late-stage 15 embryos stained with anti-GFP antibody to reveal cytoplasmic calcium detectable on GCaMP reporter binding. Calcium-dependent GCaMP signal was at a high level in control LTs (C) and comparatively weaker in $dRyR^{16}$ mutant LTs (D). Scale bar 10 μm.

## Assessing the impact of the *RYR1* undiagnosed variant mutation in *Drosophila*

*Drosophila* dRyR shares 45% aa sequence identity with human RYR1 and RYR2, and all protein domains are conserved, with up to 75% of identity for the most C-terminal RIH domain (Fig. S5A). Thus, although the 3D conformation of the *Drosophila* dRyR has not yet been established, high sequence and positional conservation of functional domains suggest that the conformation of dRyR protein is similar to that of its vertebrate counterparts. Also, the distribution of pathogenic mutations identified in human *RYR1* and *RYR2* genes (reviewed by Lanner et al., 2010), clustered in three hot spots, correlates with the positions of conserved domains. As revealed by the identity heat map (Fig. S5B) the hot spot regions of human *RYR1 and RYR2* mutations align with the most conserved portions of the *Drosophila* dRyR indicating suitability of the *Drosophila dRyR* for modeling human *RYR* gene mutations and their impact on muscular and cardiac systems.

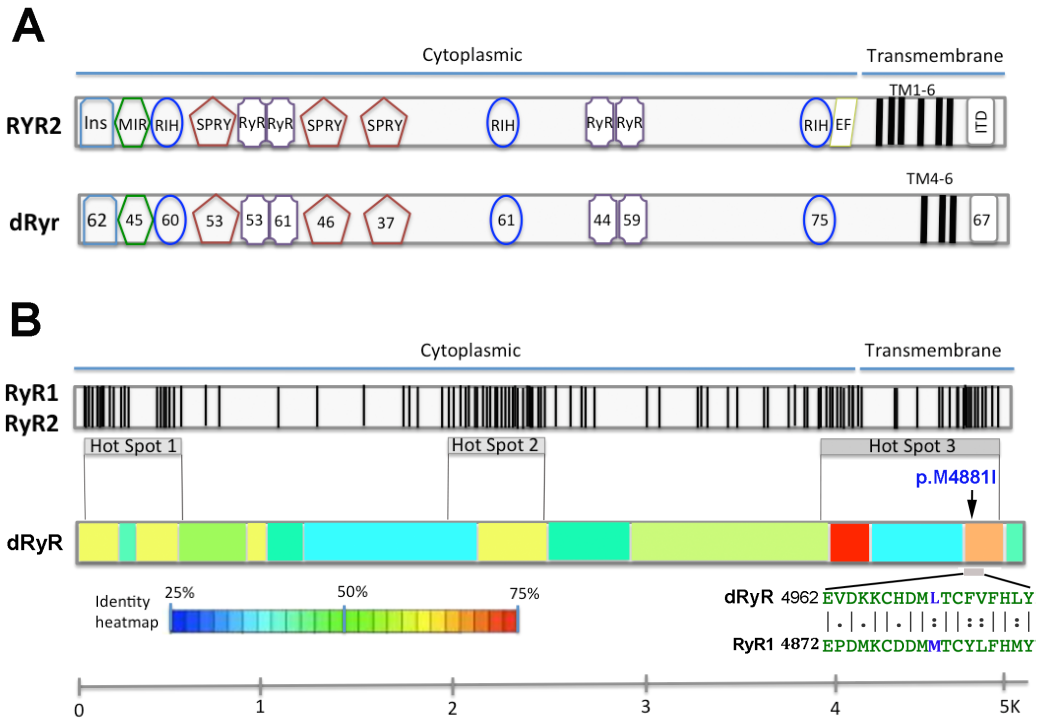


***Figure S5. Schematic comparison of amino acid sequence of human RYR and Drosophila dRyR proteins.*** (A) Schematic representation of alignment of human RYR2 and *Drosophila* dRyR proteins with focus on Ins, MIR, RIH, SPRY, RYR, EF-hand and ITD protein domains. Percentage of identity for each domain is indicated on the dRyR protein scheme. (B) Schematic representation of pathogenic mutations in human *RYR1* and *RYR2*. Black vertical lines denote positions of mutations clustered into three hot spots. For the color code, see identity heat map. Position of variant mutation of unknown significance (VUS) (p.M4881I) is indicated with respect to distribution of pathogenic *RYR* mutations and *dRyR* conservation heat map. Below an extraction from the dRyR and RYR1 sequence alignment encompassing the VUS mutation. Mutated amino acid is in blue.

Over the last decades, whole genome sequencing has identified large numbers of variant mutations within the *RYR* genes, most of which are classified as variants of unknown significance (VUS). The recessive *c.14643G>A* / p.Met4881Ile missense *RYR1* mutation was identified in a young patient

with a phenotype of congenital myopathy with a delayed acquisition of motor function. At the histopathological level, filamentous aggregates were present in muscle biopsies. This very rare mutation for which a link with a muscle disorder has not yet been evaluated, is located in the *RYR1* region encoding calcium pore.

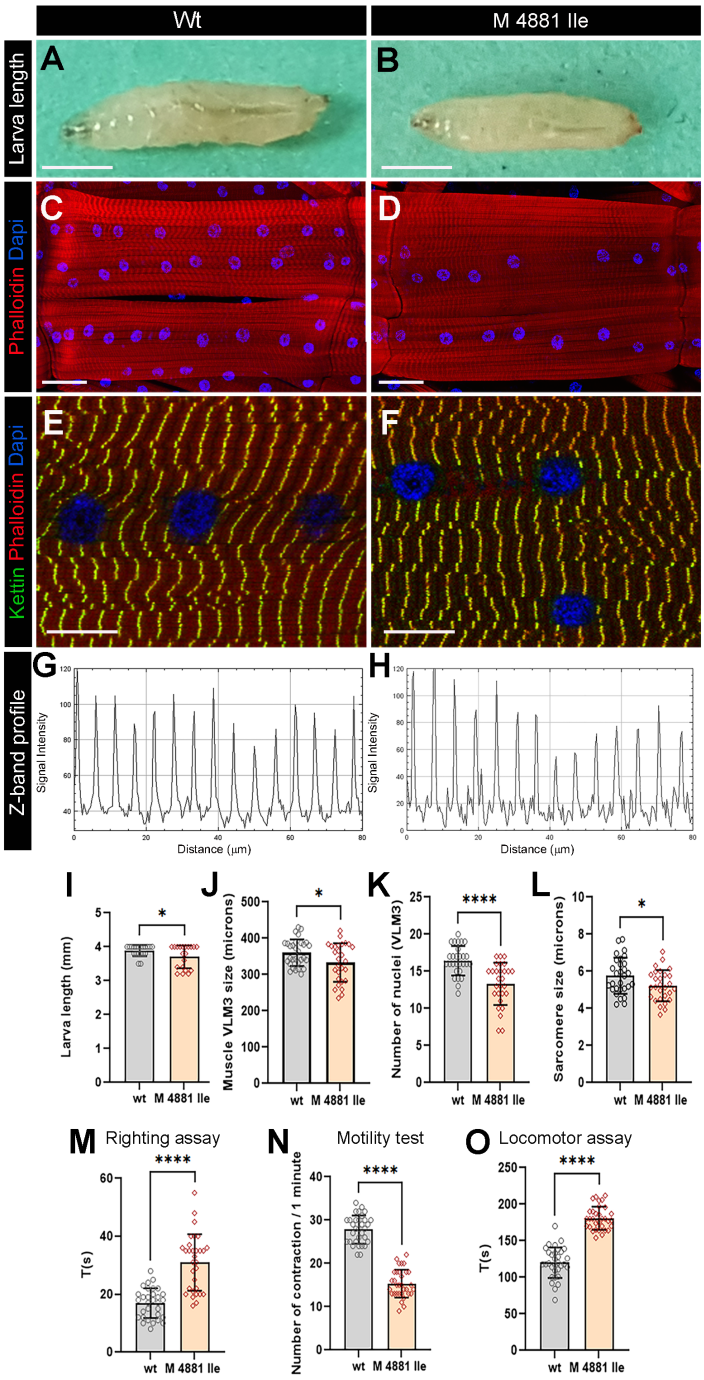


***Figure 6. Modeling human RYR1 variant mutation in Drosophila.*** (A,B) Age-matched 3rd instar wild-type (A) and *RyR1 p.Met4881Ile* mutant (B) larvae. Note a reduced size of larvae carrying *RYR1* variant mutation. (C,D) Representative views of ventral longitudinal (VL) muscles in wild type (C) and *RYR1* variant mutant larvae (D). Note slightly reduced VL3 muscle length and reduced number of myonuclei in mutant condition. (E-H) Z band profile revealing reduction of sarcomere length in *RYR1* variant context (F,H)) compared to control (E,G). Kettin is in green, Phalloidin in red and DAPI in blue. (I-L) Statistical representation of larva length (I) and structural muscle variables (J-L) in wild-type and *p.Met4881Ile RYR1* variant mutation contexts. (M-O) Statistical assessment of functional larval muscle performance using righting test (M), motility test (N) and locomotor test (O) in wild-type and *RYR1* mutant conditions. Scale bar: 1 mm in A-B; 50 mm in C-D; 20 mm in E-F. All statistical analyses were performed using Prism. The *t* test was used to compare control to variant context. Bar plot represent the mean and the standard deviation. On the figures, statistical comparisons of sample vs control are indicated as ****: P ≤ 0.0001; *: P ≤ 0.05.

We made use of the conserved muscle function and structural similarity between dRyR and human RYRs (Fig. S5A) demonstrated here to generate a *Drosophila* model of variant *p.Met4881Ile RYR1* and assess its impact on larval muscle function and structure (Fig. 6). The *p.Met4881Ile RYR1*

VUS-carrying larvae were homozygous-viable but were significantly smaller (Fig. 6B,I) than control larvae (Fig. 6A,I). They had shorter ventral longitudinal muscles (Fig. 6 D,J), which harbored fewer myonuclei (Fig. 6D,K) and were characterized by shorter sarcomeres (Fig. 6F,H) compared to control (Fig. 6C,E,G). As revealed by the larva motility tests (Fig. 6M, O) the *p.Met4881Ile RYR1* VUS impacted not only structural but also contractile muscle properties, leading to a reduced frequency of peristaltic body wall muscle contraction (Fig. 6N), slower larva locomotion (Fig. 60) and compromised muscle performance revealed by the righting test (Fig. 6M).

These structural and functional muscle phenotypes are reminiscent of those observed in *dRyR RNAi* larvae, suggesting that *p.Met4881Ile* variant mutation negatively influences *dRyR* expression and/or function and could likely contribute to RYR-related myopathies in humans.

## Discussion

The ryanodine receptors encoding calcium release channels are key regulators of intracellular calcium level, largely conserved among vertebrate and invertebrate species. By their involvement in many calcium-dependent biological processes, RYR genes are vital for normal cellular functions, while mutations in RYR genes underlie a broad spectrum of human diseases including neuromuscular and cardiac disorders (Marks, 2023). Because of their large size (over 500 kDa), structural complexity, many isoforms and broad spectrum of interacting factors, even though their role in promoting muscle contraction via E-C coupling is well-characterized, other RYR functions remain only partially understood. Here, we focus on *dRyR,* a single *Drosophila* member of the RYR gene family and characterize its expression and function in differentiated and developing muscle.

*Drosophila dRyR* shares 45% aa sequence identity with its human counterparts. Considering previous evolutionary distance studies (Ding et al., 2017) we show that the phylogenetic dRyR branch is connected to *RYR2*, the most ancient of the three human *RYRs*. Further, aa sequence alignment reveals an extensive conservation of all protein domains between *dRyR* and human RYRs, while a heatmap of conserved regions highlights previously identified hot spots of pathogenic *RYR1* and *RYR2* mutations. Remarkably, several aa residues at the functionally relevant channel pore domain (Wang et al., 2012) are conserved between *Drosophila* and humans.

Consistent with potential conservation of *dRyR* function in triggering $Ca^{2+}$ dynamics across ER membranes, we detected ER-associated punctate dRyR protein expression in differentiated body wall muscles. Our data extend previously reported analyses (Sullivan et al., 2000; Vázquez-Martínez et al., 2003) providing evidence that *dRyR* is not only expressed in visceral muscle and the nervous system but also prominently in differentiated striated somatic and cardiac muscle. We also wanted to know whether different *dRyR* transcript isoforms were differentially expressed in body wall muscles. However, we did not detect any such differential expression with 4 HCR-FISH probes targeting alternative *dRyR* exons. The fact that most *dRyR* transcript isoforms are present in differentiated larval muscles is consistent with their common transcription start sites. However, whether all *dRyR* isoforms are collectively required for larval muscle function requires further investigation. In line with muscle-associated *dRyR* expression and the excitation-contraction coupling role of its vertebrate orthologs,

RNAi knockdown of *dRyR* leads to reduced muscle contractility and severely impaired larva mobility. Interestingly, in addition to impaired muscle function, *dRyR* attenuation causes extensive structural muscle defects including reduced muscle size, smaller and aberrant sarcomeres and degraded mitochondria pattern. All these functional and structural muscle defects are reminiscent of those of aged muscle, indicating that maintenance of *dRyR*-triggered calcium management could prevent muscle aging. This applies also to cardiac muscle, which in the *dRyR RNAi* context shows aging-associated slow heart rate and arrhythmia (Blice-Baum et al., 2019).

*dRyR* transcripts and dRyR protein were also detected in the embryonic muscle precursors from embryonic stage 12 to late-stage embryos, indicating that *dRyR* could be involved in managing $Ca^{2+}$ levels throughout myogenesis. In contrast to differentiated larval muscles, HCR-FISH experiments show that only a subset of *dRyR* splice isoforms is expressed in the developing muscles. Our developmental *dRyR* expression data, focusing on somatic muscle, extend previous more general analyses of *dRyR* expression and function (Takeshima et al., 1994; Sullivan et al., 2000; Vázquez-Martínez et al., 2003). Consistent with spatiotemporal embryonic *dRyR* expression and the role of cytoplasmic calcium management (Li et al., 2025), we show that *dRyR* loss of function and RNAi knockdown in developing muscles cause severe developmental muscle defects. We found that *dRyR* promoted myogenic differentiation and was required for myotube growth associated with myoblast fusion and followed by myonuclear spreading within the myotubes. Our observations in *Drosophila* are consistent with the promoting role of *RYR1* in the calcium-dependent myoblast-to-myotube fusion process reported by the Avinoam lab in an *in vitro* myogenic differentiation system (Eigler et al., 2021). Interestingly, our analyses of embryonic muscle phenotypes of hypomorph $dRyR^{16}$ embryo reveal that *dRyR*, in addition to its major promyogenic role, may also negatively influence myogenic differentiation. A negative influence on myogenic differentiation and in particular on myoblast fusion has recently been reported in mouse *RYR1* mutant myoblast culture (Tourel et al., 2025). It was suggested that this early developmental role of *RYR1* was calcium-independent. *dRyR* might thus play a dual role in myogenesis: (i) as a calcium-independent negative regulator of first myoblast-to-myoblast fusion events and (ii) as a positive regulator of myogenic differentiation acting in later steps of myogenesis in a calcium-dependent way to promote myoblast-to-myotube fusion and muscle fiber growth. This major pro-myogenic *dRyR* function is further supported by the *dRyR* gain-of-function phenotypes.

The knowledge gained on *dRyR* and its muscle-associated functions prompted us to use *Drosophila* to test the impact of one human *RYR1* mutation with unknown significance. We chose undiagnosed recessive *p.Met4881Ile* variant mutation identified in a patient with congenital myopathy phenotypes, severely impaired mobility and accumulation of filamentous aggregates in muscle fibers. We found that *Drosophila* larvae carrying *p.Met4881Ile* mutation in the *dRyR* gene showed *dRyR RNAi*-like phenotypes with impaired larval mobility and significantly impaired sarcomeric muscle structure.
In all, we assessed eight different functional and structural muscle variables showing that *p.Met4881Ile* variant mutation consistently impaired larval muscle performance and changed muscle size and structure. This suggests that the *p.Met4881Ile* mutation impairs *dRyR* function and is likely pathogenic.

To conclude, we report functional analysis of *dRyR*, the sole fruit fly *RyR* gene and show that in addition to ensuring contractile properties of differentiated striated muscle it plays a key pro-myogenic role during muscle development. Our findings advocate *Drosophila* for modeling and testing the impact of human *RYR1* variant mutations of unknown significance.

## Materials & Methods

*Drosophila strains and genetics*

Fly stocks were maintained at 25°C on standard fly food.
The targeted expression experiments were performed using the UAS-GAL4 system (Brand and Perrimon, 1993) on the following GAL4 and UAS lines: C57-GAL4 (Bl32556); Hand-GAL4 (kindly provided by L. Perrin; TAGC, Aix-Marseille University, France); UAS-dRyR RNAi (BL29445); Lms-GAL4 (BL46861); UAS-mCherry RNAi (BL35785); UAS-dRyR (kindly provided by H. Nash University of Maryland College Park, Rockville, USA), UAS-lifeAct-GFP (BL35544), UAS-dsRed NLS (BL8547; BL8546), UAS-LacZ (BL1776), UAS-Cam RNAi (Bl34609), UAS-SERCA RNAi (BL44581) and UAS-GCaMP3 (BL32236). The $RyR^{16}$/CyO Wg LacZ (BL6812) was used as hypomorphic mutant and the $w^{1118}$ strain was used as wild type.

*Phylogenetic analysis*

Initial trees for the heuristic search were obtained automatically by applying Neighbor-Join and BioNJ algorithms to a matrix of pairwise distances estimated using the maximum composite likelihood (MCL) approach and then selecting the topology with superior log likelihood value (Kumar et al., 2018). The tree is drawn to scale, with branch lengths measured in number of substitutions per site. This analysis involved seven nucleotide sequences. Codon positions included were 1st+2nd+3rd+Noncoding. There were 17,322 positions in the final dataset.

*Immunohistochemistry*

Antibody staining was performed using standard protocol. Embryos were fixed in 4% formaldehyde and blocked in NGS serum to remove non–specific epitopes. They were incubated overnight at 4°C with primary antibodies followed by secondary antibodies for 2 h at RT.
3rd. instar larvae were dissected and fixed in 4% paraformaldehyde for 20 minutes as previously described (Lavergne et al., 2020). The fly hearts were dissected (Fink et al., 2009; Ocorr et al., 2007) and fixed for 15 min in 4% formaldehyde and the immunostaining procedure was performed as described (Auxerre-Plantié et al., 2019).
The following primary antibodies were used in this study: guinea pig anti-dRYR antibody (1:200, kindly provided by Robert Scott and Benjamin White from NIH/NIMH Institute and previously described in Gao et al., 2013), mouse anti-Dlg (1-50, DSHB, 4F3), rat anti-actin (1-500, Abcam, ab 50591), mouse anti-

kettin (1:50 DSHB 1B8-3D9), mouse anti-ATP5A (1:200 Abcam, ab 14748), goat anti-GFP (1:500, Abcam, ab 5450), and chicken anti-β galactosidase (1:1000, Abcam, ab 9361). Rhodamine phalloidin (ThermoFischer Scientific) was used to reveal actin filaments in the heart and muscles. Fluorescent secondary antibodies (Jackson ImmunoResearch) were used to detect primary antibodies.

*Muscle characteristics measurements*

All analyses of muscle length and sarcomere size were performed on fixed larval muscle preparations in a relaxed state. Acquired confocal images were analysed in Fiji using the *line tool*. *Analyze – Measure* tool was then applied to obtain muscle length values and measurements were analysed with Prism. Sarcomere size and number were calculated using *Analyze – Plot profile* Fiji tool. The sarcomere size was measured between peaks corresponding to Z-disc (revealed with Z-line specific marker) on approximatively 100 μm of muscle length. Sarcomere measurements were then analysed with Prism.
DAPI-stained nuclei were counted in Z-stacks of confocal views of VL3 larval muscle and data analysed with Prism. About 30 larval muscles from 6-8 larval filets were analysed for each measurement.

*In situ hybridization chain reaction – HCR*

In this study we used the two-stage *in situ* HCR protocol described by Choi et al. (2016). This technique detects and amplifies specific transcripts by the direct binding of probes to nucleic target sequences without additional long-lasting enzymatic reaction. We planned four different mRNA probes targeting alternative exons numbered 10,11,22 and 23.
We used a Molecular Instruments HCR kit containing a DNA probe set, a DNA HCR amplifier B1-Alexa fluor 488, B2-fluor 532 and hybridization, wash and amplification buffers.
Fixed samples were pre-hybridized at 65°C for 2 h followed by hybridization steps overnight at 45°C. After several washes, the amplification step was performed overnight at RT in the dark. We used TRJ244 HCR amplifier B1, RTJ245 HCR amplifier B2, RTJ256 HCR amplifier B2, RTJ 247 HCR amplifier B1. Target mRNA sequence information remains at the discretion of Molecular Instruments Company. Excess of hairpins was removed by several washes with 5XSSCT solution at room temperature.

*Imaging*

Samples were mounted in Vectashield with DAPI (Vector Laboratories, Inc. Burlingame, CA) and a Leica SP8 confocal microscope was used for image acquisition and for time-lapse imaging of living embryos. *In vivo* imaging of lateral muscle was performed from late stage 14 to stage 16 every 3 min. We used Adobe Photoshop and ImageJ for image processing.

*Genome editing*

To generate the *Drosophila* model of human *RYR1* VUS p.Met4881Ile we applied the CRISPR-Cas9 homologous recombination genome editing approach with the use of single strand oligo donor (ssODN) and gRNA. A 20nt 5'-AAACGCTTCGTGTTCCATCTGTAC-3' gRNA targeting the *dRYR* region close to the mutation site was designed using the OPTIMAL Target Finder platform (Gratz et al., 2014) and

cloned into PCFD5 plasmid (Adgene). Single strand ssODN donor of 115 nt in size with sequence modification TTG to ATC was generated by IDT Company. Both components were injected at a concentration of 100 ng/μl by Best Gene into nos-Cas 9 (III-attp2) flies. PCR molecular screening with a pair of primers: Forward 5'-TGCAGAGCAGCCGGAGGATGAC; Reverse 5'-ATCAGACGCGGCGAATCCGCAG and Sanger sequencing were used to identify progenies carrying the edited sequence. Genetic crosses established homozygous *Drosophila* lines carrying the RyR1 p.Met4881Ile variant mutation.

*Functional tests of muscle performance*

Motility tests were carried out on 30 3rd instar larvae as previously described (Picchio et al., 2013). The motility test was performed by recording the number of peristaltic contractions executed by the larva in 1 min on a grape medium plate. The righting test consisted in placing the larva on its back and measuring the time it took to revert to its crawling position. For the locomotor test, a track 2 mm wide, 5 mm deep and 5 cm long was prepared on a grape medium plate. Larvae were placed on the test track and the time they took to crawl a distance of 5 cm was recorded.

*Heartbeat analyses*

The cardiac activity analyses of adult Drosophila hearts were performed on 1-week-old females flies using the Semi-automated Optical Heartbeat Analysis (SOHA) approach protocol of Fink et al. (2009). For each experiment about 20 flies were analyzed. The flies were anesthetized with Fly Nap, dissected in an oxygenated, artificial hemolymph composed of 108 mM NaCl, 5 mM KCl, 2 mM CaCl2, 8 mM MgCl2 , 1 mM NaH2 PO4 , 4 mM NaHCO3, 10 mM sucrose, 5 mM trehalose, 5 mM HEPES (pH 7.1). The beating hearts were filmed by digital camera on 30s movie with the speed of 150 frames/s (Digital camera C9300, Hamamatsu, McBain Instruments, Chatsworth, CA). The SOHA program based on Matlab R2009b software was used for film analysis (Fink et al., 2009).

*Mitochondria area quantifications*

The total area of mitochondria was identified by Otsu thresholding on Fiji for internal muscle z-planes. The quantifications for z-planes were averaged for each of 25-30 different VL3 muscle according to Zhang et al., (2024).

*Statistic*

All statistical analyses were performed using Prism (v9.5.1, GraphPad, Software, La Jolla, CA, USA). The *t* test was used to compare control to variant context and one-way ANOVA tests were used for comparisons with more than two datasets. Bar plot represent the mean and the standard deviation. On the figures, statistical comparisons of sample vs control are indicated as ****: $P \leq 0.0001$; ***: $P \leq 0.001$; **: $P \leq 0.01$; *: $P \leq 0.05$; ns > 0.05.

*Ethical approval*

This study was conducted in accordance with the ethical standards of the institutional and national research committees. Ethical approval was obtained from the appropriate institutional ethics committee under the reference 38RC21.0399

## Acknowledgments

We thank Drosophila Bloomington Stock Centers for Drosophila lines and L. Mouty for the technical assistance. This study was supported by the « Priority Research Programme on Rare Diseases » of the French Investments for the Future Programme, by the AFM-Telethon strategic grant to MyoNeurAlp consortium, the Reference Centre for Neuromuscular Diseases grant to MZ and CS, ANR-iSITE-2025 grant to MZ, by the French Government Scholarship grant to MMP and The Polish National Agency for Academic Exchange within The Bekker Programme (grant no. BPN/BEK/2021/2/00006) to MDM.

## References

1. Auxerre-Plantié E, Nakamori M, Renaud Y, Huguet A, Choquet C, Dondi C, Miquerol L, Takahashi MP, Gourdon G, Junion G, Jagla T, Zmojdzian M, Jagla K. Straightjacket/α2δ3 deregulation is associated with cardiac conduction defects in myotonic dystrophy type 1. *Elife*. 2019, 8, e51114.
2. Bertin B, Renaud Y, Jagla T, Lavergne G, Dondi C, Da Ponte JP, Junion G, Jagla K. Gelsolin and dCryAB act downstream of muscle identity genes and contribute to preventing muscle splitting and branching in Drosophila. *Sci Rep.* 2021, 11(1), 13197.
3. Blice-Baum AC, Guida MC, Hartley PS, Adams PD, Bodmer R, Cammarato A. As time flies by: Investigating cardiac aging in the short-lived Drosophila model. *Biochim Biophys Acta Mol Basis Dis.* 2019, 1865(7), 1831-1844.
4. Brand AH, Perrimon N. Targeted gene expression as a means of altering cell fates and generating dominant phenotypes. *Development*. 1993, 118, 401-415.
5. Choi HM, Calvert CR, Husain N, Huss D, Barsi JC, Deverman BE, Hunter RC, Kato M, Lee SM, Abelin AC, Rosenthal AZ, Akbari OS, Li Y, Hay BA, Sternberg PW, Patterson PH, Davidson EH, Mazmanian SK, Prober DA, van de Rijn M, Leadbetter JR, Newman DK, Readhead C, Bronner ME, Wold B, Lansford R, Sauka-Spengler T, Fraser SE, Pierce NA. Mapping a multiplexed zoo of mRNA expression. *Development*. 2016, 143(19), 3632-3637.
6. De Mandal S, Shakeel M, Prabhakaran VS, Karthi S, Xu X, Jin F. Alternative splicing and insect ryanodine receptor. *Archives of Insect Biochemistry and Physiology*, 2019. *102*(3), e21590.
7. Ding Z, Peng J, Liang Y, Yang C, Jiang G, Ren J, Zou Y.. Evolution of Vertebrate Ryanodine Receptors Family in Relation to Functional Divergence and Conservation. *International Heart Journal*, 2017, *58*(6), 969–977.
8. Eigler T, Zarfati G, Amzallag E, Sinha S, Segev N, Zabary Y, Zaritsky A, Shakked A Umansky KB, Schejter ED, Millay DP, Tzahor E, Avinoam O. ERK1/2 inhibition promotes robust myotube growth via CaMKII activation resulting in myoblast-to-myotube fusion. *Dev Cell*. 2021, 56(24), 3349-3363.e6.

9. Fill M, Copello JA. Ryanodine Receptor Calcium Release Channels. *Physiological Reviews*, 2002, *82*(4), 893–922.
10. Fink M, Callol-Massot C, Chu A, Ruiz-Lozano P, Izpisua Belmonte JC, Giles W, Bodmer R, Ocorr K. A new method for detection and quantification of heartbeat parameters in Drosophila, zebrafish, and embryonic mouse hearts. Biotechniques. 2009, 46(2),101-13.
11. Fruen BR, Black DJ, Bloomquist RA, Bardy JM, Johnson JD, Louis CF, Balog EM. Regulation of the RYR1 and RYR2 Ca2+ release channel isoforms by Ca2+-insensitive mutants of calmodulin. *Biochemistry*. 2003, 42(9), 2740-7.
12. George CH, Rogers SA, Bertrand BMA, Tunwell REA, Thomas NL, Steele DS, Cox EV, Pepper C, Hazeel CJ, Claycomb WC, Lai FA. Alternative Splicing of Ryanodine Receptors Modulates Cardiomyocyte Ca $^{2+}$ Signaling and Susceptibility to Apoptosis. *Circulation Research*, 2007, *100*(6), 874–883.
13. Gao S, Sandstrom DJ, Smith HE, High B, Marsh JW, Nash HA. Drosophila ryanodine receptors mediate general anesthesia by halothane. Anesthesiology. 2013 118(3): 587-601.
14. Gratz SJ, Ukken FP, Rubinstein CD, Thiede G, Donohue LK, Cummings AM, O'Connor-Giles KM. Highly specific and efficient CRISPR/Cas9-catalyzed homology-directed repair in Drosophila. Genetics. 2014 196(4):961-71.
15. Hadiatullah H, He Z, Yuchi Z. Structural Insight Into Ryanodine Receptor Channelopathies. Front Pharmacol. 2022 23;13:897494.
16. Hasan G, Rosbash M. *Drosophila* homologs of two mammalian intracellular Ca2+-release channels: Identification and expression patterns of the inositol 1,4,5- triphosphate and the ryanodine receptor genes. *Development*, 1992,*116*(4), 967–975.
17. Howe K, Clark MD, Torroja CF, Torrance J, Berthelot C, Muffato M, Collins JE, Humphray S, McLaren K, Matthews L, McLaren S, Sealy I, Caccamo M, Churcher C, Scott C, Barrett JC, Koch R, Rauch G-J, White S, Stemple DL. The zebrafish reference genome sequence and its relationship to the human genome. *Nature*, 2013, *496*(7446), 498–503.
18. Jenden DJ, Fairhurst AS. The pharmacology of ryanodine. Pharmacol Rev. 1969, 21(1),1-25.
19. Kimura M. A simple method for estimating evolutionary rates of base substitutions through comparative studies of nucleotide sequences. *Journal of Molecular Evolution*, 1980,*16*(2), 111–120.
20. Klatt Shaw D, Gunther D, Jurynec MJ, Chagovetz AA, Ritchie E, Grunwald DJ.. Intracellular Calcium Mobilization Is Required for Sonic Hedgehog Signaling. *Developmental Cell*, 2018, *45*(4), 512-525. e5.
21. Kumar S, Stecher G, Li M, Knyaz C, Tamura K. MEGA X: Molecular Evolutionary Genetics Analysis across Computing Platforms. *Molecular Biology and Evolution*, 2018, *35*(6), 1547–1549.
22. Lanner JT, Georgiou DK, Joshi AD, Hamilton SL.. Ryanodine Receptors: Structure, Expression, Molecular Details, and Function in Calcium Release. *Cold Spring Harbor Perspectives in Biology*, 2010, *2*(11), a003996–a003996.
23. Lanner JT. Ryanodine receptor physiology and its role in disease. *Adv Exp Med Biol*. 2012, 740, 217-234.
24. Lavergne G, Zmojdzian M, Da Ponte JP, Junion G, Jagla K. Drosophila adult muscle precursor cells contribute to motor axon pathfinding and proper innervation of embryonic muscles. *Development*. 2020, 147(4)
25. Li X, Zhao X, Qin Z, Li J, Sun B, Liu L. Regulation of calcium homeostasis in endoplasmic reticulum-mitochondria crosstalk: implications for skeletal muscle atrophy. *Cell Commun Signal*. 2025, 23(1), 17.
26. Liu Q, Chen B, Yankova M, Morest DK, Maryon E, Hand AR, Nonet ML, Wang ZW. Presynaptic Ryanodine Receptors Are Required for Normal Quantal Size at the *Caenorhabditis elegans* Neuromuscular Junction. *The Journal of Neuroscience*, 2005, *25*(29), 6745–6754.
27. Mackrill JJ. (2012). Ryanodine Receptor Calcium Release Channels: An Evolutionary Perspective. In Md. S. Islam (Ed.), *Calcium Signaling* (Vol. 740, pp. 159–182). Springer Netherlands.

28. Marks AR. Targeting ryanodine receptors to treat human diseases. J Clin Invest. 2023 Jan 17;133(2):e162891.
29. Maryon EB, Coronado R, Anderson P. Unc-68 encodes a ryanodine receptor involved in regulating C. elegans body-wall muscle contraction. *The Journal of Cell Biology*, 1996, *134*(4), 885–893.
30. McKay PB, Griswold CK.. A comparative study indicates both positive and purifying selection within ryanodine receptor (RyR) genes, as well as correlated evolution: DIVERGENCE AND CORRELATED EVOLUTION OF RyRs. *Journal of Experimental Zoology Part A: Ecological Genetics and Physiology*, 2014, *321*(3), 151–163.
31. Murayama T, Kurebayashi N. Two ryanodine receptor isoforms in nonmammalian vertebrate skeletal muscle: Possible roles in excitation–contraction coupling and other processes. *Progress in Biophysics and Molecular Biology*, 2011, *105*(3), 134–144.
32. Nishimura M, Ocorr K, Bodmer R, Cartry J. Drosophila as a model to study cardiac aging. *Exp Gerontol.* 2011 (5):326-30.
33. Ocorr K, Reeves NL, Wessells RJ, Fink M, Chen HS, Akasaka T, Yasuda S, Metzger JM, Giles W, Posakony JW, Bodmer R. KCNQ potassium channel mutations cause cardiac arrhythmias in Drosophila that mimic the effects of aging. Proc Natl Acad Sci U S A. 2007, 04(10):3943-8.
34. Ottini L, Marziali G, Conti A, Charlesworth A, Sorrentino V. *α* and *β* isoforms of ryanodine receptor from chicken skeletal muscle are the homologues of mammalian RyR1 and RyR3. *Biochemical Journal*, 1996, *315*(1), 207–216.
35. Picchio L, Plantie E, Renaud Y, Poovthumkadavil P. and Jagla K. Novel *Drosophila* model of myotonic dystrophy type 1: phenotypic characterization and genome-wide view of altered gene expression. *Hum. Mol. Genet.* 2013, 22, 2795-2810.
36. Postlethwait JH, Yan YL, Gates MA, Horne S, Amores A, Brownlie A, Donovan A, Egan ES, Force, A., Gong, Z., Goutel, C., Fritz, A., Kelsh, R., Knapik, E., Liao, E., Paw, B., Ransom, D., Singer A, Thomson M, Talbot, WS.. Vertebrate genome evolution and the zebrafish gene map. *Nature Genetics*, 1998,*18*(4), 345–349.
37. Quinn KE, Castellani L, Ondrias K, Ehrlich BE. Characterization of the ryanodine receptor/channel of invertebrate muscle. *American Journal of Physiology-Regulatory, Integrative and Comparative Physiology*, 1998, *274*(2), R494–R502.
38. Sinha S, Elbaz-Alon Y, Avinoam O. Ca2+ as a coordinator of skeletal muscle differentiation, fusion and contraction. *FEBS J*. 2022, 289(21), 6531-6542.
39. Stecher G, Tamura K, Kumar S. Molecular Evolutionary Genetics Analysis (MEGA) for macOS. *Molecular Biology and Evolution*, 2020, *37*(4), 1237–1239.
40. Suisse A, Treissman JE. Reduced SERCA Function Preferentially Affects Wnt Signaling by Retaining E-Cadherin in the Endoplasmic Reticulum. *Cell Rep*, 2019, 26, 322-329.e3
41. Sullivan KMC, Scott K, Zuker CS, Rubin GM. The ryanodine receptor is essential for larval development in *Drosophila melanogaster*. *Proceedings of the National Academy of Sciences*, 2000, *97*(11), 5942–5947.
42. Takeshima H, Nishi M, Iwabe N, Miyata T, Hosoya T, Masai I, Hotta Y.. Isolation and characterization of a gene for a ryanodine receptor/calcium release channel in *Drosophila melanogaster*. *FEBS Letters*, 1994, *337*(1), 81–87.
43. Tourel A, Reynaud-Dulaurier R, Brocard J, Fauré J, Marty I, Petiot A. RyR1 Is Involved in the Control of Myogenesis. *Cells*. 2025, 14(3):158.
44. Vázquez-Martínez O, Cañedo-Merino R, Díaz-Muñoz M, Riesgo-Escovar JR. Biochemical characterization, distribution and phylogenetic analysis of *Drosophila melanogaster* ryanodine and IP3 receptors, and thapsigargin-sensitive Ca2+ ATPase. *Journal of Cell Science*, 2003, *116*(12), 2483–2494.
45. Wang J, Li Y, Han Z, Zhu Y, Xie Z, Wang J, Liu Y. Li X. Molecular Characterization of a Ryanodine Receptor Gene in the rice Leaffolder, Cnaphalocrocis medinalis. *PLoS ONE*, 2012, 7, 5, e36623

46. Wu HH, Brennan C, Ashworth R.. Ryanodine receptors, a family of intracellular calcium ion channels, are expressed throughout early vertebrate development. *BMC Research Notes*, 2011, *4*(1), 541.
47. Zhang X, Avellaneda J, Spletter ML, Lemke SB, Mangeol P, Habermann BH, Schnorrer F. Mechanoresponsive regulation of myogenesis by the force-sensing transcriptional regulator Tono. *Curr Biol.* 2024, 34(18), 4143-4159. e6.
48. Xu X, Bhat MB, Nishi M, Takeshima H. Ma J. Molecular cloning of cDNA encoding a Drosophila Ryanodine Receptor and functional studies of the Carboxyl-Terminal Calcium Release Channel. *Biophys. J*. 2000, 78, 1270-1281.